LA-UR-17-30690
Approved for public release; distribution is unlimited.

Title: Chromium (VI) reduction in acetate- and molasses-amended natural media: empirical model development

Author(s): Hansen, Scott
Boukhalfa, Hakim
Karra, Satish
Wang, Dongping
Vesselinov, Velimir Valentinov

Intended for: Report

Issued: 2017-11-21

Chromium (VI) reduction in acetate- and molasses-amended natural media: empirical model development

Scott K. Hansen, Hakim Boukhalfa, Satish Karra,
Dongping Wang, and Velimir V. Vesselinov

Los Alamos National Laboratory

October 23, 2017

Abstract

Stimulating indigenous microbes to reduce heavy metals from highly toxic oxidized species to more benign reduced species is a promising groundwater remediation technique that has already seen successful field applications. Designing such a bio-remediation scheme requires a model incorporating the kinetics of nonlinear bio-geochemical interactions between multiple species. With this motivation, we performed a set of microcosm experiments in natural sediments and their indigenous pore water and microbes, generating simultaneous time series for concentrations of Cr(VI), an electron donor (both molasses and acetate were considered), and biomass. Molasses was found to undergo a rapid direct abiotic reaction which eliminated all Cr(VI) before any biomass had time to grow. This was not found in the acetate microcosms, and a distinct zero-order bio-reduction process was observed. Existing models were found inappropriate and a new set of three coupled governing equations representing these process dynamics were developed and their parameters calibrated against the time series from the acetate-amended microcosms. Cell suspension batch experiments were also performed to calibrate bio-reduction rates in the absence of electron donor and sediment. The donor used to initially grow the cells (molasses or acetate) was found not to impact the reduction rate constants in suspension, which were orders of magnitude larger than those explaining the natural media microcosm experiments. This suggests the limited utility of kinetics determined in suspension for remedial design. Scoping studies on the natural media microcosms were also performed, suggesting limited impact of foreign abiotic material and minimal effect of diffusion limitation in the vertical dimension. These analyses may be of independent value to future researchers.

1 Introduction

Hexavalent chromium, Cr(VI), is known to be toxic to a wide variety of organisms, both single-cellular and more complex (Focardi et al., 2013). Because chromium has numerous industrial uses (Palmer and Puls, 1991), it is frequently encountered as an environmental contaminant in the subsurface at former industrial sites. Despite the general toxicity of Cr(VI), there are a variety of microorganisms that are known to be capable of reducing it to a sparingly soluble and significantly less toxic form, Cr(III). This capability has spurred interest in field-scale in-situ stimulation of indigenous microbes via nutrient injection as a method of groundwater bio-remediation.

The Cr(VI)-reducing capabilities of a variety of microbial species have been considered in the literature. These species include *Bacillus* (Cheng and Li, 2009), *Pseudomonas* (Cheng and Li, 2009), *Enterobacter* (Cheng and Li, 2009), *Escherichia coli* (Cheng and Li, 2009), *Shewanella* (Cheng and Li, 2009), *Halomonas* (Murugavelh and Mohanty, 2012), *Exiguobacterium* (Okeke, 2008), and *Providencia* (Thacker et al., 2006), among others. In addition, remediation by mixed natural microbial

cultures has also been considered (Aravindhan et al., 2007; Biradar et al., 2012; Chirwa and Wang, 2000; Das, 2009; Rehman et al., 2013; Vainshtein et al., 2003). The various microbes reduce Cr(VI) in a variety of ways. Cr(VI) is known to be enzymatically reduced under both aerobic and anaerobic conditions (Dhal et al., 2013; Focardi et al., 2013), and by reaction with microbial metabolites (Steinberger and Holden, 2005). The published laboratory work has considered the effect of a variety of different controls, including pH, initial Cr(VI) concentration, temperature, initial electron donor concentration, biomass concentration, and electron donor (Aravindhan et al., 2007; Acosta-Rodríguez and Cárdenas-González, 2010) although results are in almost all cases qualitative.

Compared to the amount of work that has been performed on qualitative behavior of various microbes and biochemical parameters on Cr(VI) reduction, less has been done on the modeling of bio-reductive transport. An early numerical approach to field-scale modeling of bioremediation introduced a three-equation model involving a mobile electron donor (assumed to be the contaminant), and oxygen (governed by the same transport equation), as well as immobile biomass (Wheeler et al., 1992). The contaminant was assumed to be consumed only in the microbial growth reaction, which was linear in biomass, Monod in donor, and Monod in electron donor. Subsequently, others (Clement et al., 1996; Suk et al., 2000) adopted similar approaches, but explicitly modeling both mobile and immobile biomass. This same general form of reaction was also adopted in a theoretical study on mixing effects(Cirpka and Valocchi, 2007).

A few field scale modeling studies have been performed on heavy metals in particular, focused on the bioremediation of uranium under anaerobic conditions at the Old Rifle Site in Colorado (Yabusaki et al., 2007; Li et al., 2010, 2011). These conceptions treat the contaminant as an electron acceptor, which implies a reduction equation, in batch, of the form

$$\frac{\partial C}{\partial t} \propto \mu, \tag{1}$$

where C $[\mathrm{mol/L}]$, is the heavy metal (Cr(VI), in our case) concentration and μ $[\mathrm{mol/s}]$ is the biomass growth reaction rate. In these models,

$$\mu = \lambda_{B_1} B \left(\frac{C}{K_C + C} \right) \left(\frac{F}{K_F + F} \right), \tag{2}$$

where λ_{B_1} $[1/\mathrm{s}]$ is an intrinsic biologically mediated reaction rate constant, B $[\mathrm{mol/L_b}]$ is the biomass concentration (The unit $[\mathrm{L_b}]$ refers to a liter of bulk volume, whereas the unsubscripted unit $[\mathrm{L}]$ refers to a liter of water), F $[\mathrm{mol/L}]$ is the electron donor or "*food*" concentration, K_C $[\mathrm{mol/L}]$ is the metal reduction Monod constant, and K_F $[\mathrm{mol/L}]$ is the electron donor Monod constant.

Cr(VI) bio-reduction is also commonly seen as an incidental, enzymatic process (under both aerobic and anaerobic conditions), in which it is not either the electron donor or the terminal electron acceptor. In this case, the above-mentioned formulations are not directly applicable. An accepted formula for enzymatic Cr(VI) biodegradation in batch is(Okeke, 2008; Wang and Shen, 1997)

$$\frac{\partial C}{\partial t} \propto B \left(\frac{C}{K_C + C} \right). \tag{3}$$

So far, none of the works mentioned derive a full system of equations for B, C, and F. A full system of governing reactive transport equations for enzymatic microbial Cr(VI) reduction has been presented by Alam (Alam, 2004), and by Shashidhar et al. (Shashidhar et al., 2007). The latter authors described the Cr(VI) degradation reaction with (1), using the following definition of μ:

$$\mu = \lambda_{B_1} B \left(\frac{K_{C'}}{K_{C'} + C} \right) \left(\frac{F}{K_F + F} \right), \tag{4}$$

where $K_{C'}$ $[\mathrm{mol/L}]$ is the Cr(VI) inhibition constant. While this equation appears superficially similar to (2), the C factor represents entirely different behavior: not as an energy source but rather as an

inhibitor. Interestingly, since μ is a proxy for the biomass growth reaction, C consumption is modeled as dependent on μ, but not vice versa. The dynamics for electron donor and biomass concentrations are both modeled straightforwardly, in terms of the biomass growth reaction:

$$\frac{\partial F}{\partial t} \propto \mu, \tag{5}$$

and

$$\frac{\partial B}{\partial t} = \mu - \lambda_{B_2} B, \tag{6}$$

where λ_{B_2} $[1/\mathrm{s}]$ is an intrinsic senescence rate, accounting for eventual biomass die-off. Alam(Alam, 2004) presented a comparatively elaborate model included transport with both mobile and immobile biomass, and also included two enzymes (both created due to biomass growth, but one conserved, and one irreversibly consumed during bio-reduction). Neglecting the irreversibly-consumed enzyme and the mobile-immobile behavior, his model can be framed, in batch, in terms of the equations we have already presented. The Cr(VI) degradation reaction in his model is (3), and the electron donor and biomass dynamics are described by (4-6).

Relatively few authors have combined modeling and experiment when studying Cr(VI) reduction. Wang and Shen(Wang and Shen, 1997) fit a two-dependent-variable model (Cr(VI) and biomass concentrations) featuring biomass death, but not accounting for biomass growth or electron donor / energy source utilization. Okeke (2008) fit a Cr(VI) Monod decay equation to determine its rate constants. Basu et al. (2014) attempted to fit a biomass growth model which assumed Cr(VI) was the energy source under apparently aerobic conditions, contrary to what might be expected. All of these experiments were performed in broth suspensions. Alam (2004) fit his model against a laboratory column experiment using initially sterilized porous media, a pure culture of *Shewanella oneidensis* MR-1 bacteria, and lactate as an electron donor. The equations of Shashidhar et al. Shashidhar et al. (2007) and minor variants were calibrated in a sequence of experiments Shashidhar et al. (2007); Somasundaram et al. (2009, 2011); Jeyasingh et al. (2011) in artifical systems (initially sterilized soil was amended with laboratory grown cultures originating elsewhere) at a variety of laboratory scales. These experiments all used molasses as an electron donor, and ignored the possibility of direct abiotic Cr(VI) reduction by molasses.

Given the environmental significance of field-scale in-situ bio-stimulation in the service of Cr(VI) reduction, it is important to have models that capture the kinetics of the interactions between electron donor, biomass, and Cr(VI) under a wide range of conditions. Since human health is at stake, it is also important to populate these models with realistic kinetic parameters. No model calibration has apparently been performed in natural geologic media in concert with its indigenous pore water and microbes, and all calibration has apparently used a set of empirical equations that assumes all biomass growth and electron donor consumption are due to the same reaction (unlikely, given the complexity of aqueous geochemistry). Furthermore, recent results published by Chen et al.Chen et al. (2015), as well as those obtained in our experiments, suggest that the presence of molasses will render an attempt to calibrate a bio-reduction model futile on account of direct, abiotic reduction.

In light of the above concerns, we started from a blank page. We performed a set of microcosm experiments in natural media and its indigenous pore water and microbes, examining the effect of two potential electron donors, acetate and molasses, on the reduction of Cr(VI). We confirmed rapid abiotic reduction by molasses prior to appearance of biomass. Using the acetate-amended microcosms, we developed a system of coupled equations that, while informed by existing formulations, significantly differed from them, and captured very well the dynamics of electron donor, biomass, and Cr(VI), while being simple enough to be meaningfully constrained by the experimental data. Using time series of concentrations from the natural media experiments, we simultaneously fit all the model parameters. We also performed another set of experiments employing cells grown with the same electron donors, which were subsequently placed into suspension in a liquid that did not contain any added electron donor or geologic media. We compared the kinetics derived from these experiments with those that were found most appropriate from the natural media experiments.

2 Materials and methods

2.1 Sample collection

Microcosm experiments were set up to monitor microbial growth in natural sediments saturated with aerobic water collected at the same site. The sediments were collected from a well drilled into a Cr(VI)-contaminated area situated in the Los Alamos Canyon in Los Alamos, NM (Vesselinov et al., 2013). Coring was performed using sonic drilling, without addition of any drilling fluids in order to preserve bio-geochemical conditions of the sediment samples. The core sample used in our study was collected from the saturated zone below the water table, at a depth below surface of between 304 and 306 m, and contained 25 wt.% moisture. After drilling, core samples were stored in sealed Lexane tubing in a refrigerated environment cooled to 4°C. Two kilograms of the core sample were collected into a sterile container and mixed to form a homogeneous sample.

The sediments used in this study were from the Miocene Pumiceous formation (Broxton and Vaniman, 2005; Vesselinov et al., 2013), consisting of reddish yellow and light gray gravel with sand and abundant silt, pumice and mixed volcanic detritus materials. The formation is dominated with 65-80 wt.% amorphous materials which consist primarily of volcanic glass or tephra derived from Pliocene volcanic events. Total feldspar content ranges from 11-35 wt.% with smectite ranging from 2-11 wt.%. In total, these three major groups are 80-94 wt.% of the samples. Mafic minerals range from 2-11 wt. % with magnetite up to 2 wt.%, augite up to 6 wt.%, and pigeonite (or Ca-enstatite) up to 3 wt.%. $\mathrm{Fe_2O_3}$ content of the samples ranged from 1.12 to 3.01 wt.%.

The pore water extracted from the sediment cores was characterized by low total organic carbon of about 0.1 mg/kg, a near-neutral pH of 7.81, an alkalinity measured as $\mathrm{CO_3^{2-} + HCO_3^-}$ = 79.37 mol, and a dissolved oxygen content of 5 to 8 mg/L. The concentration of nitrate in the samples ranged from 0.5 to 2.0 ppm, sulfate varied from 4 to 10 ppm, chloride from 5.5 to 8.5 ppm, with phosphate levels very low, in the range of 0.00 to 0.02 ppm. Cr(VI) concentration was also very low, ranging from 0.005 to 0.01 ppm. The average concentrations of other major constituents were: $\mathrm{SiO_2}$ = 31.0 ppm, Mn = 0.5 ppm, Co = 0.001 ppm, Fe = 0.21 ppm, Ca = 26.6 ppm, Mg = 7.68 ppm, Mn = 0.5, Na = 22.1 ppm, K = 4.1 ppm. Microbial cell counts on average varied between 2×10^5 and 3×10^5 cells/g of sediments.

2.2 Reduction experiments in natural media

Dozens of natural media microcosms, each in their own Petri dish, were prepared following an identical procedure. Each microcosm consisted of 32 g of sediments supplemented with an aliquot containing an electron donor (either acetate or molasses), adjusted to give a final concentration $F = 0.02$ M, 0.1 M, or 0.2 M of the electron donor in the pore water. The amended sediments were transferred to sterile Petri dishes and vibrated to form a flat sediment disk with an estimated porosity of 0.25. To facilitate microbial growth quantification, three polycarbonate sterile filters (0.22 μm, 24 mm) were deposited on top of the sediments and inoculated using a 20 μL inoculum containing ~ 10000 bacterial cells. The permeable membrane of the filters limited microbial transport between the surface of the membrane and the sediment sample but allowed free exchange of fluids and nutrients. Although the biomass was potentially restricted to one edge of the system, supporting analyses presented in Appendix A suggest that diffusion limitation across the Petri dish is not likely to affect the results for physically realistic sets of parameters. The Petri dishes containing the sediments were transferred to a plastic bag filled with argon. Sterilized water from an open container was added to the bag to saturate the air within and limit evaporation from the sediments. The bag was vacuum-emptied and refilled with argon several times to evacuate as much of the ambient oxygen as possible, and was kept under positive argon pressure for the duration of the experiment to limit oxygen diffusion back into the bag. The bag was covered with a black tarp and kept under static conditions at ambient temperature.

Sampling was performed by removing individual Petri dishes for characterization (discarding them thereafter). The membrane filters were collected using tweezers and suspended in 1.0 or 2.0 mL of saline solution (0.9% NaCl) and vortexed to suspend the biofilm in the solution. The cell numbers in the suspension were determined directly, using a cell counting hemocytometer plate. At each time point, 1.0 g of sediment was also suspended in 10 mL saline solution, vortexed, and centrifuged at 1000 rpm for 5 minutes to separate the cells from the sediment. The cell counts in the supernatant were determined by direct counting. The remaining sediments were centrifuged using Maxi-Spins centrifuge filter devices (Life Science Products) to separate the pore water from the sediments. The supernatant solutions were analyzed to quantify concentrations of electron donor, Cr(VI), sulfate, nitrate, and pH.

2.3 Reduction experiments in cell suspensions

Additional experiments were performed under controlled conditions to eliminate the effects of sediment and electron donors on Cr(VI) reduction and obtain reduction rates attributable to cell kinetic limitations alone. The experiments were performed under cell suspension conditions using cells grown anaerobically and collected at full growth. The cultures were centrifuged after two weeks, with cells harvested under anaerobic conditions using protocols described in the literature (Boukhalfa et al., 2007). The cells were washed three times to remove any remaining electron donor or other microbial metabolites, and resuspended in a saline solution. An aliquot of the cell suspension was added to a 20 mL serum vial containing 10 mL of well water spiked to 1.0 ppm Cr(VI), and without nitrate and sulfate. The concentration of Cr(VI) was monitored over time to establish its reduction rate as a function of biomass concentration. Cell numbers remained constant during these experiments.

Concentrations of Cr(VI) were analyzed spectrophotometrically using a modification of EPA method 7196A (USEPA, 1986–2015). A solution of 1,5-diphenylcarbazide was prepared by dissolving 0.02 g in 100 mL deionized water, acidified with 5 mL of 1.0 M HCl. This solution was then mixed in equal volume with a solution containing unknown amounts of Cr(VI). The solutions were left to equilibrate for 10 min before reading their absorbance at 542 nm, which was correlated to the concentration of Cr(VI) using a calibration curve produced using Cr(VI) standards. This method is very sensitive and can achieve detection limits in the low ppb range. Acetate concentration was analyzed using a Dionex Summit HPLC using procedures available in the literature (Duke et al., 2007). The flow rate was 0.5 mL/min and the mobile phase was composed of 30 mM $\mathrm{KH_2PO_4}$ (pH = 2.57) in a 40% (v/v) methanol aqueous solution. The column used was a C18 Acclaim 120 (Thermo Scientific). Absorbance was measured at 222 nm. Acetate standards were analyzed by ion chromatography (IC) following EPA method 300 (USEPA, 1983) on a Dionex DX-600 system. Molasses concentrations were analyzed using EPA method 415.3 (Potter and Wimsatt, 2005). A calibration curve was established by measuring the TOC of solutions with known concentrations of molasses. The method is sensitive at the ppm level.

3 Results

3.1 Microbial growth and electron donor consumption

Biomass growth data in Figure 1A show a significant and rapid increase in the biomass for both acetate and molasses. The ultimate cell density is significantly greater than what one might expect under strict anaerobic conditions, indicative of the availability of oxygen to the microbial cells (the natural pore water used in our experiments contains 5 to 8 mg/L oxygen and was not degassed prior to the incubation). The evolution of biomass growth is typical and shows a short period of slow growth during the incubation period, followed by rapid growth, with the biomass concentration approximately stabilizing after about two weeks (Figure 1A). Late time overall biomass content appears similar

for all three initial electron donor concentrations considered. The rate of consumption/decay of the electron donor appears approximately proportional to its concentration, rather than to the biomass concentration (Figure 1C).

3.2 Kinetics of Cr(VI) reduction in natural media

In the sediments stimulated by molasses, Cr(VI) concentrations decreased very rapidly, to the point that its concentration was non-detect at the the first observation time, after 50 hours (Figure 1B). Despite the early Cr(VI) depletion, data continued to be collected on the molasses and biomass concentrations for 15 days, and these are shown in Figure 1A,C. It is notable that Cr(VI) disappeared before any biomass growth was detected, precluding bio-reduction as a plausible pathway. In this case, it is most likely that molasses reduced the Cr(VI) abiotically, either through a direct aqueous reaction, or by reducing an intermediary which in turn reduced the Cr(VI). This is consistent with recent literature which documents abiotic Cr(VI) reduction by molasses (Chen et al., 2015). Notably, only a small amount of molasses was required to completely remove the Cr(VI). On account of the apparent abiotic reaction, it was not sensible to calibrate a model which is predicated on bio-reduction against this data.

In the sediments stimulated by acetate, the situation was distinctly different. For all three time series of acetate-amended sediments, Cr(VI) concentration dropped immediately (i.e., by the time of the first measurement) by approximately 50%, and then remained roughly constant for a few days, beginning to decrease as biomass appeared. We attributed the rapid early-time reduction to foreign particles that were introduced during collection of the natural media (see analyses in Appendices B and C). The Cr(VI) decrease once the biomass grew was relatively slow and approximately zero-order, for all time series. The zero-order kinetics suggest a saturated catalyst (in this case a bio-catalyst, above its Monod threshold), and appear to preclude a direct aqueous reaction with acetate. Note also that acetate consumption is approximately first order. Abiotic reaction catalyzed by sediments cannot be ruled out, although direct reaction *transforming* the sediments (after the initial decrease) again seems implausible in light of the order of the kinetics. The onset of the late-time zero-order decay corresponding to the appearance of biomass renders bio-reduction the parsimonious explanation for the late-time tailing.

3.3 Kinetics of Cr(VI) reduction in cell suspensions

The data in Figure 2A show Cr(VI) reduction versus time for a variety of suspensions with different cell concentrations and cells grown using both molasses and acetate. No particular pattern is apparent relating the decay rate to the electron donor with which the cells were initially grown. Decay appears to be generally exponential, reflecting first-order kinetics. The rapid Cr(VI) decay shows that microbial cells are effective at reducing Cr(VI) even though no electron donors were added to the suspension. This has been previously described for several metal-reducing microorganisms (Fredrickson et al., 2000) and it has been referred to as endogenous respiration. This process is attributed to the availability of energy sources within the cells, which they obtained during their growth phase (Boukhalfa et al., 2007).

4 Discussion

4.1 Model development

We developed a set of coupled equations relating the variables B, C, and F to explain the acetate-amended microcosm time series. The biomass dynamics were determined by a growth rate, $\lambda_{B_1}[\mathrm{mol/L_b/s}]$,

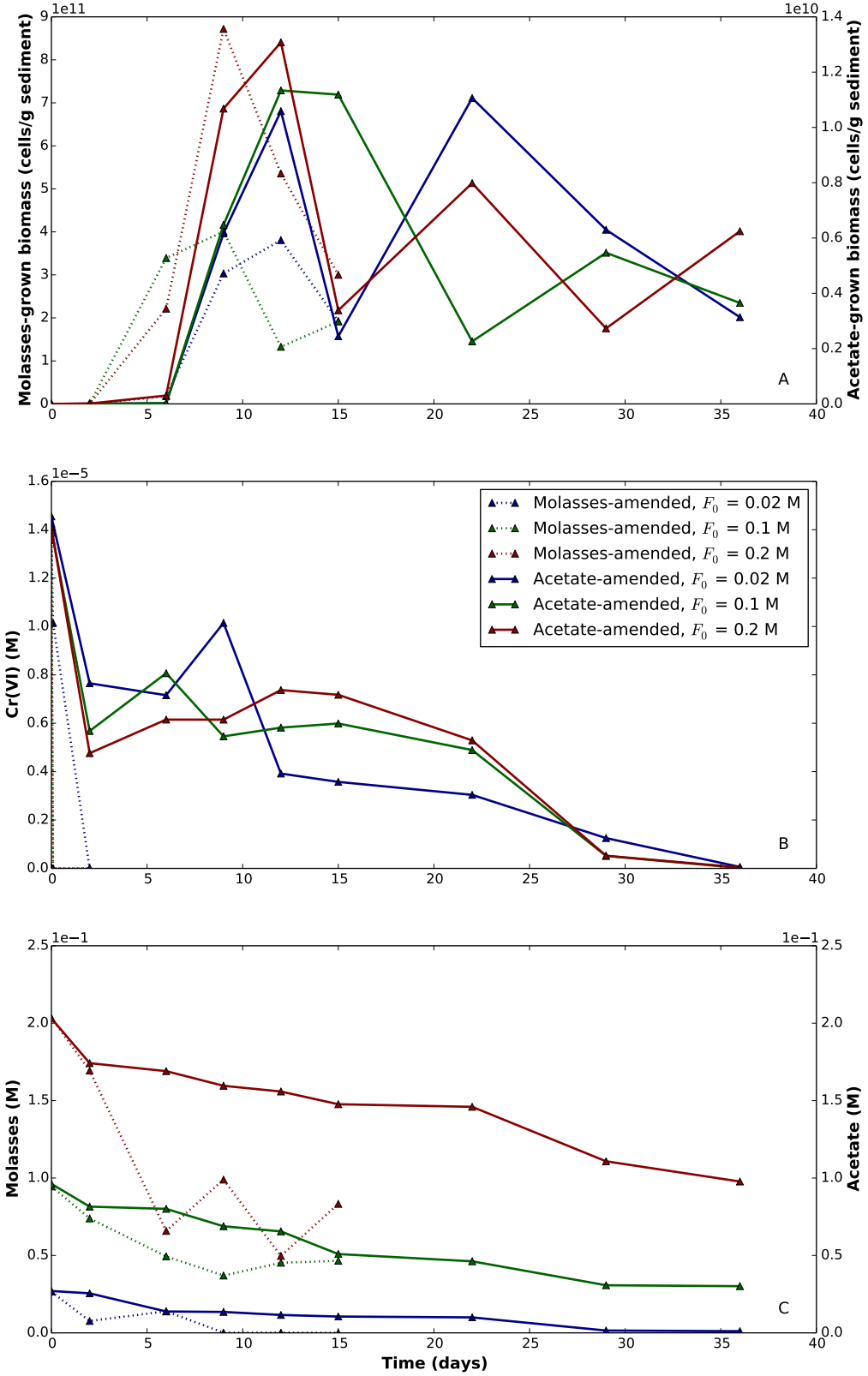

Figure 1: Concentration time series from the natural media reduction experiments, for each initial electron donor concentration, F_0, and for both electron donors: (A) biomass density, B, (B) Cr(VI) concentration, C, and (C) electron donor concentration, F. Legend applies to all axes.

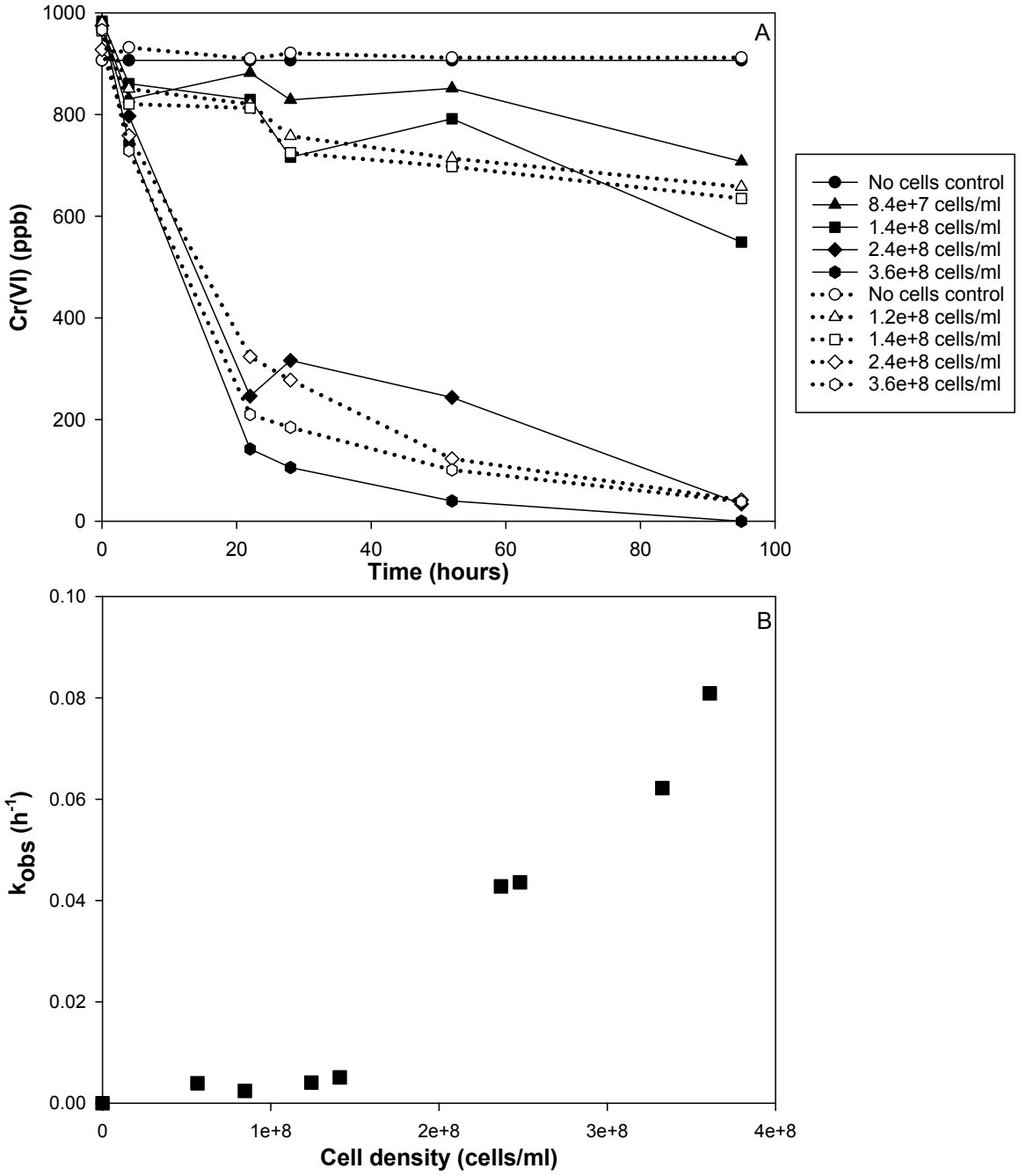

Figure 2: Concentration time series and best-fit decay rate constants from cell suspension experiments. (A) Reduction of Cr(VI) concentrations in various suspensions with different cell concentrations (under non-growth conditions). The dotted time series are for cells grown with acetate, and the solid time series are for cells grown with molasses. (B) First-order Cr(VI) decay rate constants fit for each time series on the top axes, as a function of the concentration in the cell suspensions.

and also by a senescence rate λ_{B_2} $[1/\mathrm{s}]$:

$$\frac{\partial B}{\partial t} = \lambda_{B_1}\left(\frac{B}{K_B + B}\right) - \lambda_{B_2} B \qquad \left[\frac{\mathrm{mol}}{\mathrm{L_b\ s}}\right]. \tag{7}$$

The biomass production rate was taken to be proportional to the biomass concentration for low biomass concentrations (a classic exponential growth model), with an inhibition term causing the growth rate to tail off to a constant value for high concentrations. Compared to the work of Alam (2004), the inhibition term due to growth is new, but considered essential for practical modeling of bio-remediation. Furthermore, in the time series, the concentration of the added electron donor was not found to play a role in controlling the biomass growth rate (possibly because it had a Monod form, as in Alam (2004), and electron donor concentration in all the experiments was above the cutoff concentration). While there must plainly be a Monod-type dependence of biomass growth on electron donor concentration, this form could not be constrained by our time series data. Consequently, the effect of donor availability was simply subsumed into the effective rate constant, λ_B.

The Cr(VI) reduction dynamics were determined according to the standard enzymatic Monod relation (3):

$$\frac{\partial \theta C}{\partial t} = -\lambda_C B\left(\frac{C}{K_C + C}\right) \qquad \left[\frac{\mathrm{mol}}{\mathrm{L_b\ s}}\right], \tag{8}$$

with rate constant λ_C $[1/\mathrm{s}]$, Monod constant K_C $[\mathrm{mol/L}]$, and porosity θ.

Food consumption was governed by rate constant λ_F $[1/\mathrm{s}]$, representing the number of moles of food consumed per mole of biomass produced, as well as kinetics. Again, a form which is Monod in electron donor, with Monod constant K_F $[\mathrm{mol/L}]$, was seen as most appropriate, reflecting a finite metabolic capacity of the biomass:

$$\frac{\partial \theta F}{\partial t} = -\lambda_F B\left(\frac{F}{K_F + F}\right) \qquad \left[\frac{\mathrm{mol}}{\mathrm{L_b\ s}}\right]. \tag{9}$$

This governing equation differs most strongly from the existing approaches of Alam (2004) and Shashidhar et al. (2007) (eqs. 4 and 5). These approaches took electron donor consumption to be proportional to the biomass growth, and this was definitely not the case in our experiments. The electron donor consumption was found only to be dependent on its own concentration, suggesting it was consumed largely by reactions other than those driving biomass growth.

4.2 Model calibration

4.2.1 Cr(VI) reduction in acetate-amended natural media

To extract parameters from the time series for acetate-amended sediments, model calibration was performed by simultaneously fitting all of the model parameters in (7-9) to best match the three time series (one for each of B, C, and F) for each of the three initial acetate concentrations ($F_0 =$ 0.02 M, 0.1 M, and 0.2 M) by iterative parameter perturbation (Vesselinov et al., 2016; Vesselinov and O'Malley, 2016). As mentioned above, apparent abiotic reaction was observed, but restricted to early time. Consequently, the first two points of each acetate time series shown in Figure 1 were discarded, and calibration was performed on the last 30 days worth of data. Comparison of the model predictions for each of B, C, and F, for the optimized parameters and the corresponding subset of the raw data are shown in Figure 3. Optimized parameter values are displayed in Table 1.

4.2.2 Cr(VI) reduction in cell suspensions

The cell suspension experiments showed approximately exponential decay for a range of cell concentrations (Figure 2A) and, as mentioned, no discernible pattern regarding the media in which the

Table 1: Optimized parameter values for (7-9), yielding the model predictions shown in Figure 3.

λ_{B_1}	4×10^{-3}	$\left[\mathrm{mol\,L_b^{-1}\,s^{-1}}\right]$
λ_{B_2}	1×10^{-5}	$\left[\mathrm{s^{-1}}\right]$
K_B	5×10^{1}	$\left[\mathrm{mol\,L_b^{-1}}\right]$
λ_C	2.25×10^{-15}	$\left[\mathrm{s^{-1}}\right]$
K_C	1×10^{-7}	$\left[\mathrm{mol\,L^{-1}}\right]$
λ_F	2.25×10^{-11}	$\left[\mathrm{s^{-1}}\right]$
K_F	3×10^{-2}	$\left[\mathrm{mol\,L^{-1}}\right]$

cells were grown prior to being put into suspension. By linear regression of time against the logarithm of the Cr(VI) concentration for each time series, first-order rate parameters were computed. These are plotted against biomass concentration numbers for each suspension in Figure 2B. A mild upward curvature is apparent, although a zero-intercept straight line, consistent with the model developed for the microcosm experiments, can be fit unproblematically. Because biomass concentration was constant in each suspension and first-order decay was detected, it follows that the Monod constant for the batch reaction must satisfy $K_C \gg 2 \times 10^{-5}$ M (as this was the approximate initial Cr(VI) concentration in the suspensions). Using (8) as the interpretive framework, the quantity on the vertical axis of Figure 2B represents $\frac{1}{C}\frac{dC}{dt}$, and the quantity on the horizontal axis represents B. Converting B to units of $\mathrm{mol\,L^{-1}}$, the best-fit zero-intercept regression line between B and $\frac{1}{C}\frac{dC}{dt}$ has slope $8\times10^{-7}\mathrm{L\,mol^{-1}\,s^{-1}}$, implying $\frac{\lambda_C}{K_C} = 8\times10^{-7}\mathrm{L\,mol^{-1}\,s^{-1}}$. Based on our constraint on K_C, this implies that $\lambda_C \gg 1.6 \times 10^{-11}$. Both the λ_C and K_C derived from the cell suspension batch experiments are higher by orders of magnitude from those most applicable to the experiments performed in natural media, listed in Table 1.

4.3 Joint discussion of experiments and models

In the microcosms amended with acetate, Cr(VI) was reduced steadily, with a zero-order late-time tail. Bio-reduction processes were seen to be the parsimonious explanation for this behavior, and a set of coupled ordinary differential equations was developed to model the bio-reduction dynamics. While acetate was consumed in accordance with a Monod rate law, there was no evidence that reduction in the amount of available acetate in the system reduced the rate of growth of the biomass. Indeed, the best kinetic model of biomass growth was found not to explicitly depend on acetate concentration. This is an interesting asymmetry, and suggests that electron donor was largely consumed by the biomass for other purposes than growth, which differs from existing models. Further, despite evidence that Cr(VI) reduction was biologically driven, the rate constant for Cr(VI) reduction was orders of magnitude smaller than that for acetate oxidation, suggesting that biologically-mediated electron transport from acetate to Cr(VI) was a comparatively unimportant pathway as far as acetate consumption is concerned, unlike the model of Shashidhar et al. Indirect reduction by a bacterial metabolite is a possibility (Priester et al., 2006; Steinberger and Holden, 2005).

In the microcosms amended with molasses, Cr(VI) was reduced almost immediately, before biomass appeared. This suggests a direct, rapid reaction between a constituent of molasses and Cr(VI). A bio-reduction model was obviously not appropriate for these systems. While these experiments were "unsuccessful" as far as calibrating bio-reduction rate parameters, the rapid direct reaction is actually promising from a contaminant remediation standpoint, and field-scale in-situ remediation is a large motivator for exploration of bio-stimulated Cr(VI) reduction. This aligns with

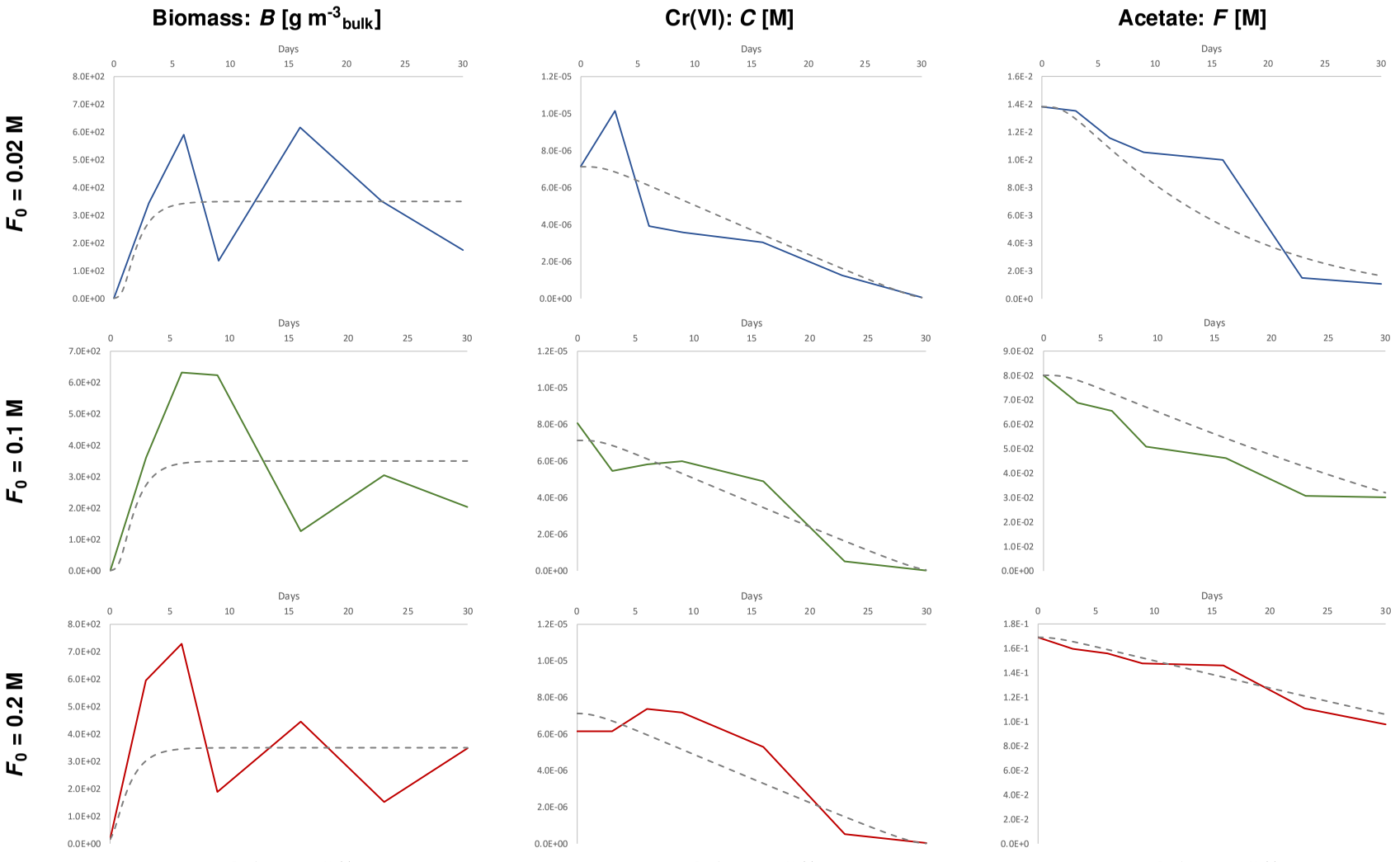

Figure 3: Comparisons of experimental data (solid lines; colored as in Figure 1) and calibrated model predictions (dashed lines) for each of B, C, and F, for each of three separate experimental batches which were initialized with a different amount of acetate $F_0 \equiv F(0)$. Each row is devoted to a different batch, and each column is devoted to a different species. In all the plots, the vertical axis represents concentration. For Cr(VI) and acetate, this is molar. Biomass concentrations are denominated in $\mathrm{g/m^3_{bulk}}$. Parameters yielding the model predictions are shown in Table 1

the recent results of Chen et al. (2015), and goes against the classic conception of molasses as a bio-stimulant only.

The cell suspension experiments, when interpreted with the model found optimal for the acetate-amended natural media microcosm experiments, yielded K_C and λ_C which were orders of magnitude larger than those calibrated from the natural media microcosms. Interestingly, this disparity existed despite the fact that there should not be global-scale diffusion limitation when the natural media is treated as 1D (Appendix A). Reasons for this are not entirely clear, and more study would be needed to resolve this. A possibility is that there was actually diffusion limitation in 3D, with localized blobs of biomass, as this is seen to impose a more severe limitation (Appendix B). Regardless of the underlying reason, this experience suggests that care must be taken in the usage of batch-derived bio-reduction kinetics for field-scale in-situ remediation problems—even at the centimeter scale.

Substantial variability in biomass concentrations was observed between subsequent points in any single time series, despite effort going into identical preparation of the various microcosms. This suggests a large inherent unpredictability when using models to predict field bio-reduction performance, and a benefit to using substantial numbers of replicates in the lab.

Going forward, the model we developed and calibrated can be used as a foundation for field-scale numerical site studies. Our results suggest strongly that all environmentally-oriented experimental studies of bio-reduction should be performed in natural media, and the limited utility of model parameters estimated based on cell-suspension experiments. Future studies exploring a wider range of model parameters and determining the functional relationship between λ_{B_1} and F would be of great practical use. In light of its apparent efficiency, the remedial use of molasses to abiotically reduce Cr(VI) also appears worthy of study.

References

Focardi, S.; Pepi, M.; Focardi, S. E. *Biodegradation - Life of Science*; 2013; pp 321–347.

Palmer, C. D.; Puls, R. W. *Natural Attenuation of Hexavalent Chromium*; 1991; pp 1–12.

Cheng, G.; Li, X. Bioreduction of chromium (VI) by Bacillus sp. isolated from soils of iron mineral area. *European Journal of Soil Biology* **2009**, *45*, 483–487.

Murugavelh, S.; Mohanty, K. Bioreduction of hexavalent chromium by free cells and cell free extracts of Halomonas sp. *Chemical Engineering Journal* **2012**, *203*, 415–422.

Okeke, B. C. Bioremoval of hexavalent chromium from water by a salt tolerant bacterium, Exiguobacterium sp. GS1. *Journal of Industrial Microbiology and Biotechnology* **2008**, *35*, 1571–1579.

Thacker, U.; Parikh, R.; Shouche, Y.; Madamwar, D. Hexavalent chromium reduction by Providencia sp. *Process Biochemistry* **2006**, *41*, 1332–1337.

Aravindhan, R.; Sreeram, K. J.; Rao, J. R.; Nair, B. U. Biological removal of carcinogenic chromium(VI) using mixed Pseudomonas strains. *The Journal of General and Applied Microbiology* **2007**, *53*, 71–79.

Biradar, N. V.; Sindagi, A. S.; Reddy, J.; Ingalhalli, S. S. Bioremediation of Chromium in Pulp and Paper Processing Industrial Effluents by Indigenous Microbes. *Journal of Bioremediation and Biodegradation* **2012**, *03*.

Chirwa, E. N.; Wang, Y. T. Simultaneous chromium (VI) reduction and phenol degradation in an anaerobic consortium of bacteria. *Water Research* **2000**, *34*, 2376–2384.

Das, A. P. Bioreduction Based Bioremediation of Hexavalent Chromium Cr(VI) Through Potential Indigenous Microbes. Ph.D. thesis, National Instituite of Technology, 2009.

Rehman, Y.; Rizvi, F. Z.; Faisal, M.; Hasnain, S. Arsenic and chromium reduction in co-cultures of bacteria isolated from industrial sites in Pakistan. *Microbiology* **2013**, *82*, 428–433.

Vainshtein, M.; Kuschk, P.; Mattusch, J.; Vatsourina, A.; Wiessner, A. Model experiments on the microbial removal of chromium from contaminated groundwater. *Water Research* **2003**, *37*, 1401–1405.

Dhal, B.; Thatoi, H. N.; Das, N. N.; Pandey, B. D. Chemical and microbial remediation of hexavalent chromium from contaminated soil and mining/metallurgical solid waste: a review. *Journal of Hazardous Materials* **2013**, *250-251*, 272–91.

Steinberger, R. E.; Holden, P. A. Extracellular DNA in single- and multiple-species unsaturated biofilms. *Applied and Environmental Microbiology* **2005**, *71*, 5404–5410.

Acosta-Rodríguez, I.; Cárdenas-González, J. F. Hexavalent chromium removal by a Paecilomyces sp. fungal strain isolated from environment. *Bioinorganic Chemistry and Applications* **2010**, *2010*.

Wheeler, M. F.; Roberson, K. R.; Chilakapati, A. Three-Dimensional Bioremediation Modeling in Heterogeneous Porous Media. University of Colorado 9th International Conference on Computational Methods in Water Resources. Denver, CO, 1992; pp 1–19.

Clement, T. P.; Hooker, B. S.; Skeen, R. S. Numerical Modeling of Biologically Reactive Transport Near Nutrient Injection Well. *Journal of Environmental Engineering* **1996**, *122*, 833–839.

Suk, H.; Lee, K.-K.; Lee, C. H. Biologically reactive multispecies transport in sanitary landfill. *Journal of Environmental Engineering* **2000**, *126*, 419–427.

Cirpka, O. A.; Valocchi, A. J. Two-dimensional concentration distribution for mixing-controlled bioreactive transport in steady state. *Advances in Water Resources* **2007**, *30*, 1668–1679.

Yabusaki, S. B.; Fang, Y.; Long, P. E.; Resch, C. T.; Peacock, A. D.; Komlos, J.; Jaffe, P. R.; Morrison, S. J.; Dayvault, R. D.; White, D. C.; Anderson, R. T. Uranium removal from groundwater via in situ biostimulation: Field-scale modeling of transport and biological processes. *Journal of Contaminant Hydrology* **2007**, *93*, 216–235.

Li, L.; Steefel, C. I.; Kowalsky, M. B.; Englert, A.; Hubbard, S. S. Effects of physical and geochemical heterogeneities on mineral transformation and biomass accumulation during biostimulation experiments at Rifle, Colorado. *Journal of Contaminant Hydrology* **2010**, *112*, 45–63.

Li, L.; Gawande, N.; Kowalsky, M. B.; Steefel, C. I.; Hubbard, S. S. Physicochemical heterogeneity controls on uranium bioreduction rates at the field scale. *Environmental science & technology* **2011**, *45*, 9959–66.

Wang, Y. T.; Shen, H. Modelling Cr(VI) reduction by pure bacterial cultures. *Water Research* **1997**, *31*, 727–732.

Alam, M. Bioreduction of hexavalent chromium: flow-through column experiments and reactive transport modeling. Ph.D. thesis, Washington State University, 2004.

Shashidhar, T.; Bhallamudi, S. M.; Philip, L. Development and validation of a model of bio-barriers for remediation of Cr(VI) contaminated aquifers using laboratory column experiments. *Journal of Hazardous Materials* **2007**, *145*, 437–452.

Basu, S.; Dasgupta, M.; Chakraborty, B. Removal of Chromium (VI) by Bacillus subtilis Isolated from East Calcutta Wetlands, West Bengal, India. *International Journal of Bioscience, Biochemistry and Bioinformatics* **2014**, *4*, 7–10.

Somasundaram, V.; Philip, L.; Bhallamudi, S. M. Experimental and mathematical modeling studies on Cr(VI) reduction by CRB, SRB and IRB, individually and in combination. *Journal of Hazardous Materials* **2009**, *172*, 606–617.

Somasundaram, V.; Philip, L.; Bhallamudi, S. M. Laboratory scale column studies on transport and biotransformation of Cr(VI) through porous media in presence of CRB, SRB and IRB. *Chemical Engineering Journal* **2011**, *171*, 572–581.

Jeyasingh, J.; Somasundaram, V.; Philip, L.; Bhallamudi, S. M. Pilot scale studies on the remediation of chromium contaminated aquifer using bio-barrier and reactive zone technologies. *Chemical Engineering Journal* **2011**, *167*, 206–214.

Chen, Z.-F.; Zhao, Y.-S.; Zhang, J.-W.; Bai, J. Mechanism and Kinetics of Hexavalent Chromium Chemical Reduction with Sugarcane Molasses. *Water, Air, & Soil Pollution* **2015**, *226*, 1–9.

Vesselinov, V. V.; Katzman, D.; Broxton, D.; Birdsell, K.; Reneau, S.; Vaniman, D.; Longmire, P.; Fabryka-Martin, J.; Heikoop, J.; Ding, M.; Hickmott, D.; Jacobs, E.; Goering, T.; Harp, D.; Mishra, P. Data and Model-Driven Decision Support for Environmental Management of a Chromium Plume at Los Alamos National Laboratory. WM2013 Conference Proceedings. Phoenix, 2013.

Broxton, D. E.; Vaniman, D. T. Geologic framework of a groundwater system on the margin of a rift basin, Pajarito Plateau, north-central New Mexico. *Vadose Zone Journal* **2005**, *4*, 522–550.

Boukhalfa, H.; Icopini, G. A.; Reilly, S. D.; Neu, M. P. Plutonium (IV) Reduction by the Metal-Reducing Bacteria Geobacter metallireducens GS15 and Shewanella oneidensis MR1. *Applied and Environmental Microbiology* **2007**,

USEPA, *Test Methods for Evaluating Solid Waste, Physical/Chemical Methods*; 1986–2015.

Duke, C. L.; Roback, R. C.; Reimus, P. W.; Bowman, R. S.; McLing, T. L.; Bake, K. E.; Hull, L. C. Elucidation of flow and transport processes in a variably saturated system of interlayered sediment and fractured rock using tracer tests. *Vadose Zone Journal* **2007**,

USEPA, *Methods for Chemical Analysis of Water and Wastes*; 1983.

Potter, B. B.; Wimsatt, J. C. *Method 415.3 - Measurement of Total Organic Carbon, Dissolved Organic Carbon and Specific UV Absorbance at 254 nm in Source Water and Drinking Water*; 2005.

Fredrickson, J. K.; Kostandarithes, H. M.; Li, S. W.; Plymale, A. E.; Daly, M. J. Reduction of Fe(III), Cr(VI), U(VI), and Tc(VII) by Deinococcus radiodurans R1. *Applied and Environmental Microbiology* **2000**, *66*, 2006–2011.

Vesselinov, V. V.; O'Malley, D.; Lin, Y.; Hansen, S. K.; Others, MADS.jl: Model Analyses and Decision Support in Julia. 2016; http://mads.lanl.gov/.

Vesselinov, V. V.; O'Malley, D. Model Analysis of Complex Systems Behavior using MADS. AGU Fall Meeting. San Francisco, CA, 2016.

Priester, J. H.; Olson, S. G.; Webb, S. M.; Neu, M. P.; Hersman, L. E.; Holden, P. A. Enhanced Exopolymer Production and Chromium Stabilization in Pseudomonas putida Unsaturated Biofilms. *Applied and Environmental Microbiology* **2006**, *72*, 1988–1996.

Appendix A: Analysis of 1D diffusion limitation of bio-reduction

As discussed in the main text body, the microcosms were constructed so that bacteria was introduced only on the upper edge, and this is also the only location where bacterial samples were collected. Consequently, an analysis was performed to assess the potential for Cr(VI) concentration gradients developing across a microcosm to reduce the effective reaction rate in the worst case: reaction restricted to the upper edge.

We solved a 1D diffusion system, where D is a Fickian diffusion constant, x is distance from bottom of the Petri dish, L is the thickness of the puck of cuttings in the dish, and λ is an effective reaction rate. The governing equation,

$$\frac{\partial C}{\partial t} = D\frac{\partial^2 C}{\partial x^2}, \tag{10}$$

was solved subject to the initial-boundary conditions

$$C(x,0) = C_0, \tag{11}$$

$$\frac{\partial C}{\partial x}(0,t) = 0, \tag{12}$$

$$D\frac{\partial^2 C}{\partial x^2}(L,t) = -k\left(\frac{C(L,t)}{K_C + C(L,t)}\right). \tag{13}$$

These conditions represent constant initial concentration, no flux through the bottom of the dish, and the simultaneous applicability of the diffusion equation and a first-order decay equation at the top surface. The diffusion constant used for Cr(VI) was $3\times10^{-9}\ \left[\mathrm{m^2\ s^{-1}}\right]$. L was assumed to be 1×10^{-2} m, and a variety of values of k were considered.

We considered the possibility of diffusion limitation under two conditions: high concentrations ($C_0 \gg K_C$), under which the RHS of (13) $\approx k$, and low concentrations ($C_0 \ll K_C$), at which RHS $\approx kC(L,t)/K_C$. For the large initial concentration simulation, RHS was approximated as $-k_1$, with values of $k_1 > \lambda_C B(L,\infty) \approx 7\times10^{-13}\ \left[\mathrm{mol\,L_b^{-1}\,s^{-1}}\right]$ explored. This baseline was chosen because the the point reaction rate at a favorable location must be at least as large as that of the reactor as a whole. For the low initial concentration, the RHS was approximated as $-k_2C(L,t)$, with values of $k_2 > \lambda_C B(L,\infty)/K_C \approx 7\times10^{-6}\ \left[\mathrm{s^{-1}}\right]$ were explored. In both cases exploration proceeded by implicit finite difference numerical analysis of system evolution for 30 days.

In high-concentration initial conditions it was found impossible generate a significant concentration gradient across the dish for a wide range of possible values of k_1. Under low-initial-concentration conditions, values of k_2 large enough to generate a noticeable gradient across the puck thickness are sufficient to yield complete degradation of Cr(VI) over time scales significantly shorter than those observed in the lab. An example of this is shown in Figure 4.

Thus, we conclude that diffusion limitation due to restriction of reaction to the edge of the domain is not apt to have been an important concern in the analysis.

Appendix B: Analysis of 3D diffusion limitation of abiotic reduction by individual particles

We consider the rate of consumption over time due to a single, instantaneously-Cr(VI)-reducing particle of radius r_p embedded at the origin of an infinite domain of initial concentration C_0. As above, the only mass transport process considered is diffusion, so we employ the 3D diffusion equation under spherically-symmetric conditions. This can be expressed in one spatial coordinate, the radial distance, r. For simplicity, we instead analyze the complimentary problem, namely

$$\frac{\partial C}{\partial t} = \frac{D}{r^2}\frac{\partial}{\partial x}\left(r^2\frac{\partial C}{\partial x}\right), \tag{14}$$

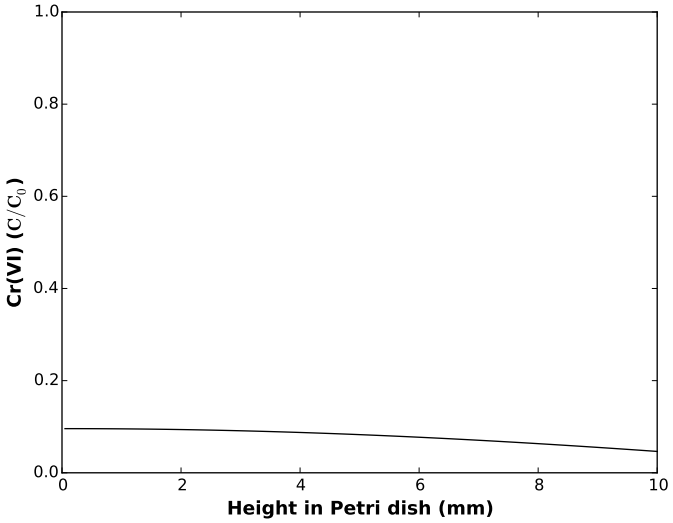

Figure 4: Profile of relative concentration across dish after one day, for low-initial-concentration case. Note the vast majority of Cr(VI) has been reduced already. Here, $k_2 =$ 3.6e-5 s^{-1}.

subject to the initial-boundary conditions

$$C(r,0) = 0 \qquad (r > r_p), \tag{15}$$

$$C(r_p,t) = C_0, \tag{16}$$

$$C(\infty,t) = 0. \tag{17}$$

The rate of change of the total amount of mass in the domain outside the particle in this complimentary problem has the same magnitude as the instantaneous rate of mass consumption by the particle. By solving this problem numerically (we assume $D = 3\times10^{-9}\left[\mathrm{m}^2\,\mathrm{s}^{-1}\right]$, and $r_p = 5\times10^{-5}\ [\mathrm{m}]$), we see that this drops to nearly zero after approximately six hours (Figure 5).

The system we are solving also admits a steady-state solution,

$$C(r,\infty) = C_0\left(\frac{r_p}{r}\right), \tag{18}$$

from which we can see (Figure 6) that the radius of influence of each particle of naturally-reducing material is on the order of millimeters: small relative to the microcosm scale. The numerical solution can also be seen to give essentially the same profile after 1 day as after all time. We take this analysis to confirm that the effect of any stationary particles causing local abiotic reduction becomes negligible over a short time.

This analysis also suggests that biomass growth which is localized in 3D in a given microcosm may lead to reduced effective bio-reduction rates relative to batch conditions. This stands in striking contrast to the 1D analysis of Appendix A, which indicated that a uniform-in-top-view sheet of biomass restricted to the edge of the Petri dish was not apt to yield significant diffusion limitation of bio-reduction.

Appendix C: supporting experiments on abiotic reduction

We noted rapid initial reduction of Cr(VI) before measurable biomass grew in the acetate-amended natural media microcosms, which was not observed in the cell suspension batch experiments. We

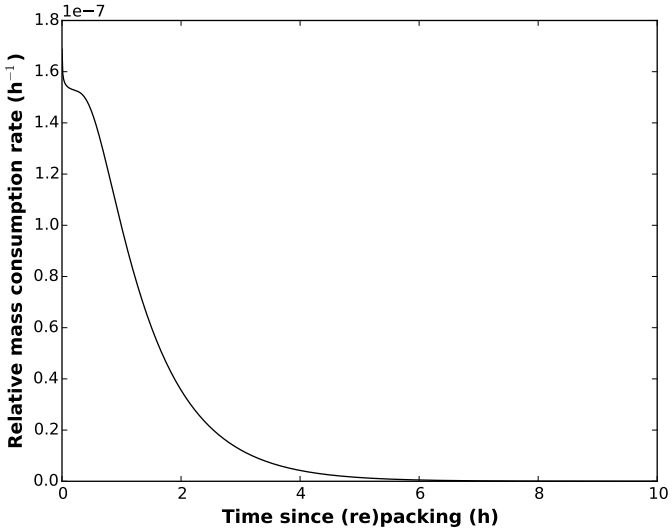

Figure 5: Relative Cr(VI) reduction rate as function of time after placement of a single spherical reducing particle inside an infinite, isotropic, uniform medium. Reaction rate computed from numerical solution of (14-17).

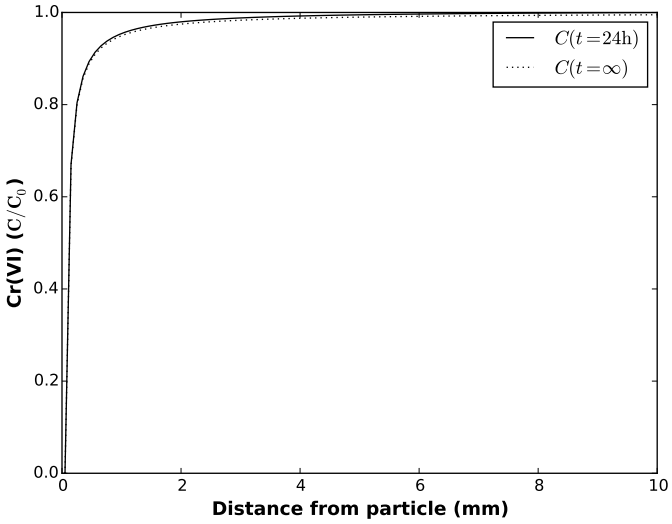

Figure 6: Concentration as a function of distance from a single, spherical reducing particle, as computed using (14-17). Results are shown after 24 hours, and at late time.

hypothesized that this early-time reduction behavior was due to reaction with abiotically reducing particles which were introduced to the natural media samples during drilling, as the existence of such strongly reducing material in the aquifer itself was not consistent with background Cr(VI) concentrations in the aquifer at the sampling location. The analysis presented in Appendix B suggests that if the early-time reduction were due to such abiotically-reducing particles then it should manifest itself as a near-instantaneous drop in Cr(VI) concentrations in the microcosms, and have limited impact thereafter. In addition, while zero-order late-time kinetics made it unlikely, it was prudent to exclude the possibility of a direct reaction between Cr(VI) and acetate analogous to the reaction observed between Cr(VI) and molasses.

To quantify these two effects, we collected two additional time series on microcosms in natural media. These microcosms were handled in identical fashion to those used to collect the bio-stimulated time series, except with these major differences:

1. Sediments were initially sterile.

2. Instead of being discarded after centrifuging and measurement, the Petri dishes were re-packed (i.e. a single dish was used for each of the two time series).

The two microcosms discussed in this appendix differed only in that one was amended with acetate, and one was not. For each microcosm, Cr(VI) concentration measurements were tabulated at four times over the course of 18 days, with results shown in Figure 7.

To within estimated experimental error, the time series were not distinct, which strengthens our supposition that there is no significant direct reaction between Cr(VI) and acetate.

Repacking the Petri dishes after each measurement was designed to test the supposition of rapid Cr(VI) reduction by foreign particles, followed by a diffusion-limited regime of negligible reduction. Since repacking "resets the clock" by spatially homogenizing Cr(VI) concentrations without regard for abiotically-reducing particle locations, we would expect to see more rapid reduction than was seen in the undisturbed microcosms discussed in Section 3 in both of the initially sterile microcosms, as they were repeatedly repacked. Furthermore, we would expect to see similar fractional Cr(VI) concentration drops between sequential repacking events, regardless of the time elapsed between them, as long as this time was > 6 h (per the analysis in Appendix B). By consulting the graphs in Figure 7, we see that these predictions are satisfied. To within experimental error, each repacking event is associated with a roughly 50% drop in Cr(VI) concentration. These microcosm studies corroborate our supposition that the only abiotic reaction in the acetate-amended microcosms is with foreign particles, and its effect in the main microcosm studies is limited to early time.

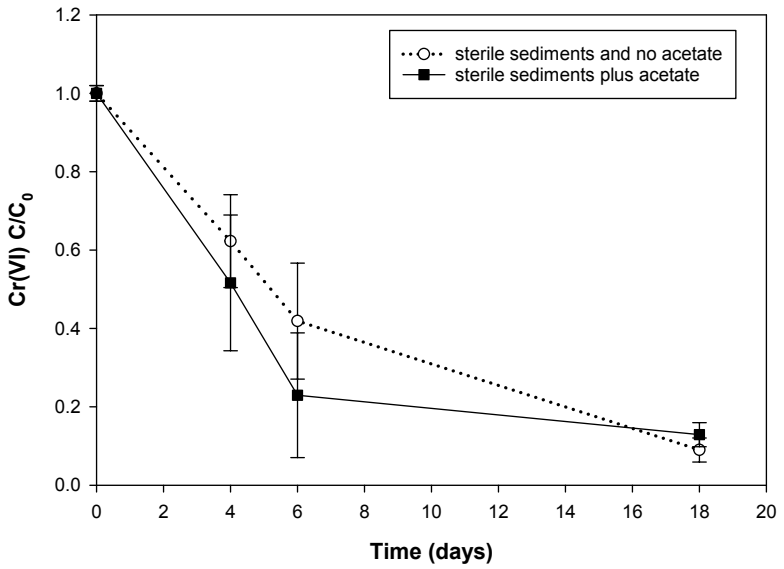

Figure 7: Cr(VI) concentration over time in two sterilized microcosms which were re-packed after each measurement. The solid line represents a microcosm with acetate initially present, and the dotted line